

Original papers

LCTF-based multispectral fluorescence imaging: System development and potential for real-time foreign object detection in fresh-cut vegetable processing



Santosh Lohumi ^a, Byoung-Kwan Cho ^{a,b,*}, Sangdeok Hong ^c

^a Department of Biosystems Machinery Engineering, College of Agricultural and Life Science, Chungnam National University, 99 Daehak-ro, Yuseong-gu, Daejeon 34134, South Korea

^b Department of Smart Agriculture System, College of Agricultural and Life Science, Chungnam National University, Daejeon, South Korea

^c Department of Quality Assurance, Samsung Welstory INC, Seongnam, Gyeonggi-do, South Korea

ARTICLE INFO

Keywords:

Fluorescence multispectral imaging
Liquid crystal tunable filter
Foreign materials
Fresh-cut vegetables
On-line detection

ABSTRACT

Ensuring the supply of safe and contaminant-free fresh-cut vegetables is of importance to consumers and suppliers worldwide. The present research aimed to develop an online inspection system, making use of fluorescence and color imaging for detection of potential foreign materials (FMs) unintentionally added to fresh-cut vegetables. A multispectral fluorescence imager incorporating a liquid crystal tunable filter (LCTF) was developed to sequentially acquire selected band images of fresh-cut vegetables. Custom-built software was developed to synchronize the LCTF with the camera exposure to collect the fluorescence images of selected spectral bands and to collect the digital color images of the same samples using a color camera. Image processing algorithms were developed for both fluorescence and color images to detect a wide range of potential FMs in two different fresh-cut vegetables, namely, cabbage and green onion. The obtained results showed that the combined use of the multispectral fluorescence technique and color imaging can detect most FMs with accuracy > 95%; however, non-fluorescent tiny dark FMs could not be detected. The potential of the developed online detection system was further tested in an industrial environment by installation in a fresh-cut processing unit. All hardware parts were enclosed in a black box and the software program was modified to programmatically control conveyor belt movement and facilitate real-time image processing for FM visualization. FMs mixed with fresh-cut vegetables were manually fed onto the conveyor belt; fluorescence and color images of fresh-cut vegetables were acquired simultaneously while moving through the conveyor belt. The developed online system performed almost identically in the industrial environment, and has the potential to scan an area as large as $24 \times 24 \text{ cm}^2$ in approximately 1.5 s. Thus, its application in commercial setting may be feasible.

1. Introduction

Food safety remains a critical issue, and is thus receiving increasing attention in both developed and developing countries. Food safety considerations involve a wide range of factors, including physical, chemical, and biological contaminations, where particular concerns of

physical contamination are fecal contamination and the presence of a range of foreign materials (Feng & Sun, 2012). The majority of consumer complaints in food-safety-related issues involve physical contamination where foreign bodies are present in food. Different types of foreign materials can be accidentally present in food. In some cases, these relate to a specific manufacturing problem, but in others they may be related to

Abbreviations: LCTF, Liquid crystal tunable filter; FMs, foreign materials; UV, Ultraviolet; HIS, hyperspectral imaging; MSI, multispectral imaging; AOTF, acousto-optic tunable filter; VIS-NIR, visible and near infrared; FOV, field of view; AOV, angle of view; FFD, flange focal distance; CCD, charge couple device; sCMOS, scientific complementary metal-oxide semiconductor; LED, light emitting diode; SDK, software development kit; NI, National instruments; VI, virtual instrument; PET, polyethylene terephthalate; PP, polypropylene; ABS, acrylonitrile-butadienestyrene copolymer; HDPE, high-density polyethylene; LDPE, low-density polyethylene; ANOVA, analysis of variance; PCA, principal component analysis.

* Corresponding author at: Department of Biosystems Machinery Engineering, College of Agricultural and Life Science, Chungnam National University, 99 Daehak-ro, Yuseong-gu, Daejeon 34134, South Korea.

E-mail address: chobk@cnu.ac.kr (B.-K. Cho).

<https://doi.org/10.1016/j.compag.2020.105912>

Received 17 June 2020; Received in revised form 15 November 2020; Accepted 21 November 2020

Available online 5 December 2020

0168-1699/© 2020 Elsevier B.V. All rights reserved.

the way in which different types of food products are sold or are used by consumers. Among the wide range of food products susceptible to foreign materials, fresh-cut vegetables are prominent, and can be contaminated by different kinds of foreign materials. A comprehensive report on food associated with incidents of foreign material contamination showed that vegetables and vegetable products attracted the most complaints for the presence of foreign materials, accounting for about 20% of foreign material contaminated events of all food products (Edwards & Stringer, 2007). These foreign materials are usually hard and sharp objects, such as different kinds of plastic pieces, wood, glass, metal, stone, and insect parts, which are accidentally added to fresh-cut vegetables during processing.

The presence of unwanted plastic pieces and other foreign materials in fresh-cut vegetables is a frequent source of complaint by consumers globally (Edwards & Stringer, 2007; Francis et al., 2012). Such incidents have a direct economic impact, as well as effects on consumers' health, which may include injuries. Thus, implementing proper inspection systems to ensure the safety of products is crucial with respect to consumer satisfaction and health, and is always required by food safety regulations.

To address the issue of foreign material detection in different kinds of food products, a range of techniques have been utilized. These techniques include metal detectors, X-ray inspection, color imaging (optical detectors), microwave imaging, terahertz imaging, ultrasonic imaging, and thermal imaging (Lee et al., 2012). However, these different techniques have been exploited for different samples and their performance depends upon the sample characteristics, such as density, color, water content, and temperature interference. Of these above-mentioned techniques, only metal detection, X-ray inspection, and color imaging have widespread commercial use; while terahertz imaging is still in the early stage of development particularly for food inspection. The advantages and disadvantages of these techniques for detecting foreign bodies in food are well reviewed and presented in (Mohd Khairi et al., 2018).

However, despite the seriousness of the issue of repeated occurrences of foreign materials in fresh-cut vegetables, no research work has been conducted to exploit the potential of the above techniques for detection of foreign materials in fresh-cut vegetables. However, considering the types of foreign materials in fresh-cut vegetables (Edwards & Stringer, 2007), the above techniques do not seem effective because the X-ray-based technique is unsuitable for detecting soft foreign materials, metal detectors can detect only metallic objects. Terahertz imaging is limited by its low spatial resolution and highly attenuated in water media (G. Kim et al., 2012; Mohd Khairi et al., 2018). In addition, a color camera-based machine vision technique may not be effective for optically opaque (plastic) foreign materials, and cannot detect foreign materials that are chromatically similar to the fresh-cut vegetables or the conveyor background.

In this work, an alternative approach using fluorescence imaging was applied to detect various foreign materials in fresh-cut vegetable processing. Recently, a system with ultraviolet (UV) excitation light has shown that fluorescence imaging could be a useful tool in the detection of foreign materials in cotton (Mustafic et al., 2014). Our basic assumption was that the most plastics would show strong signs of fluorescence at different wavebands when illuminated with UV-A (365 nm) light because some widely used commercial plastics contain additives with a significant fluorescence emission, such as optical brighteners. In addition, the leafy green vegetables naturally show a distinct chlorophyll peak in red or far red region of electromagnetic spectrum when illuminated with UV-A light. These considerations may help discriminating such contaminants from the fresh-cut vegetables. By considering the unique advantages of fluorescence imaging, a line-scan hyperspectral fluorescence imaging system that collects different spectral band images in a non-invasive manner has been utilized successfully for detection of contaminants in fruits and vegetables (Everard et al., 2014; M. S. Kim et al., 2002). In the past decade, the potential of line-

scan hyperspectral imaging (HSI) in both reflectance and fluorescence mode has been evaluated extensively for agro-food quality analysis (Feng & Sun, 2012). Although visible-near infrared (VIS/NIR) HSI has been applied to real-time quality inspection applications (Mo et al., 2017; Park et al., 2011), the use of fluorescence HSI has been mostly limited to laboratory-based studies because, unlike VIS/NIR HSI, fluorescence HSI usually requires higher exposure time, which limits its implementation for real-time applications when samples are moving through a conveyor unit. In such cases, area or plane scanning multispectral imaging (MSI) can be suitable for high-throughput fluorescence MSI, as it acquires different wavelengths sequentially for the whole scene, thus allowing the collect of the selected spectral band images from a relatively large area (several cm²) within a second.

In the past, multispectral imaging for area scanning was performed using a limited number of bandpass filters mounted on a wheel that was rotated mechanically to place the chosen wavelength filter in the optical path of the imaging camera. These systems were constrained by the slow filter switching speed, limited filter number, and the large size of the filter wheel (Evans et al., 1998). More recent developments have led to the design of electronically tunable filters, such as the acousto-optic tunable filter (AOTF) and liquid crystal tunable filter (LCTF), which respond to an applied acoustic field and electronic voltage, respectively, to select a spectral band at high speed (Abdlaty et al., 2018; Lapray et al., 2014), thus allowing the selected waveband image to be captured. Compared to the AOTF, the main advantages of the LCTF include its compactness, larger apertures and fields of view, flexible throughput control, and low power requirement (Evans et al., 1998). A small aperture due to the size of the crystal used in the AOFT inhibit its use for macro-scale imaging.

Recently, LCTF-based spectral imaging systems in both VIS and NIR wavelength ranges have been developed for quality analysis of a range of agro-food products in which only the effective wavelengths are inspected. They have been used in the prediction of the constituent concentration of single maize kernels (Cogdill et al., 2006), differentiation of different wheat classes (Mahesh et al., 2008), detection of insect-damaged wheat kernels (Singh et al., 2009), early detection of rotten citrus (Gómez-Sanchis et al., 2008), identification of sour skin infected onions (Wang et al., 2012a), and detection of chilling injury in cucumbers (Lu & Lu, 2020). Although the LCTF-based hyperspectral imaging system is appealing to some agro-food research laboratories, none have evaluated its potential for fluorescence imaging. Moreover, all of the above works were laboratory based, and the potential of LCTF-based spectral imaging systems has yet to be tested in an industrial environment for food quality and safety analysis. A possibility arises from the use of a nearly uniform wide field fluorescence light for an area scanning spectral imager synchronized with a programmable motion controller-based conveyor unit.

Thus, the overall goal of this study was to develop an online system for real-time inspection of potential FMs in a fresh-cut vegetable processing line. To achieve this, an LCTF-based spectral imager was used to collect the hyperspectral images of fresh-cut vegetables and foreign materials. The effective wavelength images were then selected to reduce the image acquisition time, data dimensionality, and computation time. A color camera was further installed to collect color images of FMs for detection of non-fluorescent and colorful foreign materials which can be overlooked in fluorescence imaging. Image processing algorithms were developed and incorporated into a custom-built software interface. As the final goal, by synchronizing the sensing units with conveyor belt movement, the foreign material detection performance of the system was investigated in an industrial environment.

2. Materials and methods

2.1. LCTF-based spectral imager

The LCTF is an optical band pass filter whose center wavelength is

electrically tunable. A typical LCTF-based spectral imager consists of the LCTF, objective lens, and area scan camera and an optional relay lens. Based on the arrangement of the above components, an LCTF-based imager can be constructed in three possible ways, as shown in Fig. 1; however, each layout has some advantages and limitations.

Layout-I, as shown in Fig. 1(a), is the most common layout for a LCTF-based imager where the LCTF is placed in front of the objective lens. The main advantage of this layout is its instrumental simplicity; however, it could result in serious mechanical vignetting due to reduction of light transmission at the edges of the lens because of the small aperture size of the LCTF. Moreover, this layout limits the field of view (FOV) because the LCTF has a limited acceptance angle of view (AOV), typically 12–15°. Hence, layout-1 cannot be considered effective when a large area (FOV) is to be scanned, as in the case of machine vision applications.

The optical layout can be altered to increase the FOV of the LCTF-based imager by placing the objective lens in front of the LCTF as shown in Fig. 1(b). However, in layout-II, an objective lens with long flange focal distance (FFD) is required to focus the objects onto the focal plane array (FPA) of the camera (Wang et al., 2012b). In our case, the LCTF thickness is 48.5 mm, thus an objective lens with FFD > 50 mm is necessary to collect the images effectively. Moreover, the FOV of the objective lens should be in accordance with the acceptance angle of LCTF. Unfortunately, such machine vision lenses are not readily available commercially. Only a small number of lenses offer such a long FFD in conjunction with a large focal length (>70 mm). However, an objective lens with large focal length cannot be used for a machine vision system, particularly when a large FOV (several cm²) is of interest.

Thus, relay lens can be used to extend the focal length and FFD of the lens, as shown in Fig. 1(c). This layout-III addresses several challenges,

including significant image vignetting and smaller FOV associated with Layout-I, and extends the FFD and allows easy focus adjustment to combat the limitations of layout-II. However, the main concern with this layout (i.e., relay lens-based) is the extra design cost and size of the spectral imager.

The ultimate objective of this work is to develop a machine vision-based system to collect multispectral images, free of vignetting, of a wide area (>20 × 20 cm²). Therefore, we require a larger aperture and AOV than the aperture diameter of the LCTF (20 mm) and AOV (12°), respectively. Hence, in this study, we considered layout-III for the development of an LCTF-based spectral imager.

2.2. Instrument design

The LCTF-based spectral imager configured based on layout-III is shown in Fig. 2c. The major components of the imaging system are the area scan camera, LCTF optical head and controller, objective lens, relay lens, illumination source, and computer unit. Since the imaging system was developed for fluorescence imaging, instead of using a conventional charged coupled device (CCD) camera, a scientific complementary metal-oxide semiconductor (sCMOS) camera (pco.panda 4.2, Kelheim, Germany) was preferred. The main advantage of a sCMOS- compared to a CCD-based camera is higher quantum efficiency with low readout noise (Tutt et al., 2014), which is an important factor to be considered in low level fluorescence imaging. The used monochrome sCMOS camera (2048 × 2048 pixels, 6.5 μm pitch, thus the sensor size is 18.8 mm diagonal) can collect 16-bit images in the spectral range of 400–1000 nm with a quantum efficiency of up to 80%. The camera was linked to the computer through a USB 3.1 interface.

The Kurios-WB1 LCTF (Thorlabs. Inc.) has an aperture size of 20 mm

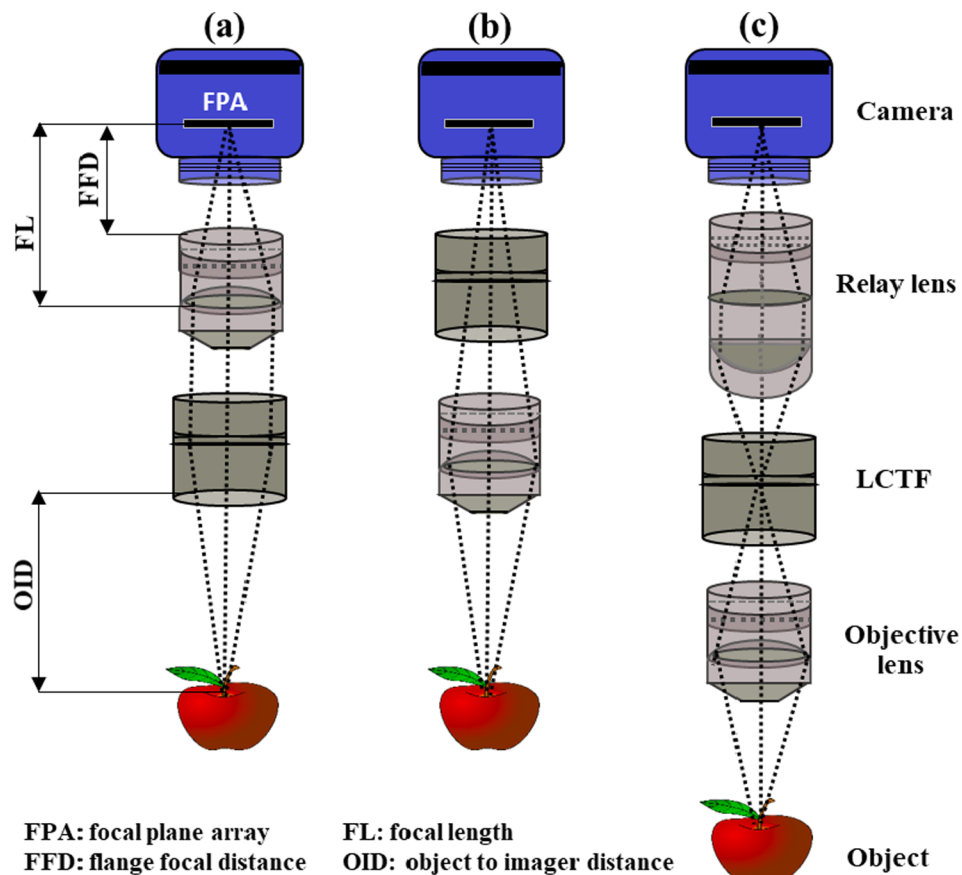


Fig. 1. Three potential layouts for the liquid crystal tunable filter (LCTF)-based spectral imaging system: (a) the LCTF is placed in front of the objective lens, (b) the LCTF is placed behind the objective lens, and (c) the LCTF is placed between the objective lens and the relay lens.

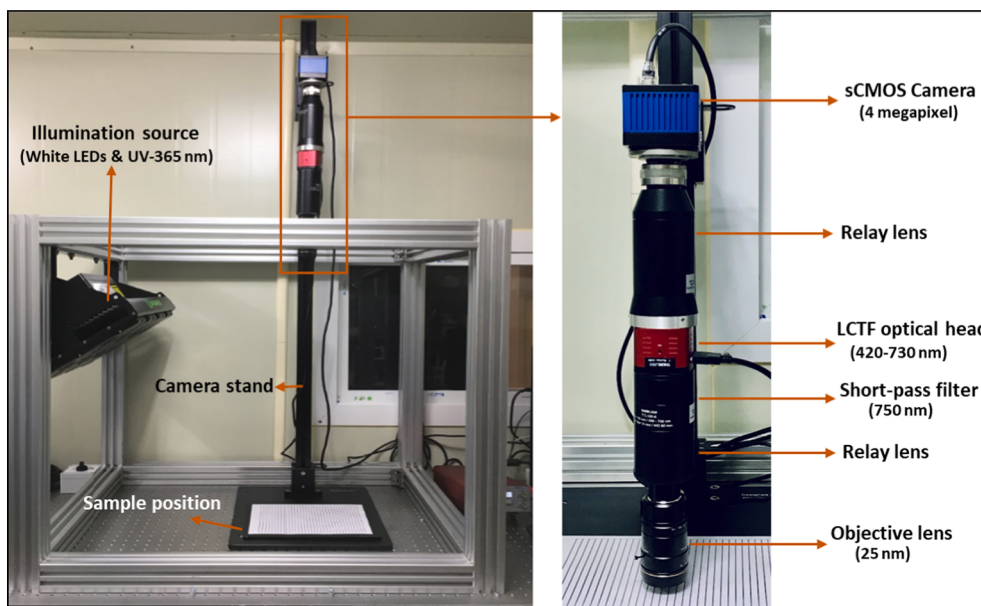


Fig. 2. Photograph of the LCTF-based spectral imaging system (left) and the sensing unit (right).

and the bandwidth at 550 nm was 35 nm with 45% transmission efficiency. The LCTF optical head is electrically tunable through an LCTF controller for rapid selection of any wavelength in the visible range (420–730 nm) with a minimum 1 nm interval and can be switched from minimum (420 nm) to maximum (730 nm) wavelength in less than 50 ms. The LCTF optical head was connected to the controller via a cable, and the controller was connected to the computer through a USB cable for software or command-line control.

A custom-designed relay lens (Channel Systems, MB, Canada), which creates an infinity space for LCTF between the objective lens and camera sensor, was used. The relay lens comprises two fully enclosed optical tubes of a combined length of approximately 30 cm. The relay lens has a C-mount objective lens interface with a fine focus adjuster, and supports up to 21 mm diagonal sensors. One tube of the relay lens connected the LCTF to the camera and the other tube connected the LCTF to the objective lens. A C-mount objective lens (Kowa Optimed GmbH, Dusseldorf, Germany) with a 25 mm focal length and maximum aperture of f/2.0 was attached to the relay lens as shown in Fig. 2. The selected objective lens has high transition efficiency in the visible range (400–750 nm) and can support a 25 mm diagonal camera sensor. In addition, a 750 nm short pass filter was incorporated before the LCTF to cut any infrared radiation reaching the LCTF and causing heat generation.

The most critical part of the machine vision or spectral imaging systems is illumination. The illumination should be nearly uniform throughout the FOV of the imaging system and result in consistent spectral outputs in the course of scanning. Unlike line-scan spectral imaging, an LCTF-based area scan imaging system requires area lighting. The LCTF-based imager developed in this work has the potential to be used for reflectance imaging by illuminating samples with white LEDs or for fluorescence imaging using ultraviolet (UV) illumination. Therefore, a commercially available illumination unit (ST700, Magnaflux, IL, USA) was used to project an ultra-wide, nearly even beam of UV-A (365 nm) light onto the inspection area and facilitate the changeover option with built-in white light. Thus, a single illumination unit could be used for both reflectance and fluorescence imaging purposes.

2.3. Software interface design

In this work, LabVIEW was used as a graphical programming language to develop a user-friendly software interface for synchronizing the

LCTF with camera exposure to collect the spectral images for each changing waveband. LabVIEW provides tools for instrumental control, data acquisition, data processing and analysis, and various modes of viewing. The software interface for the LCTF-based spectral imager, as shown in Fig. 3, was developed using LabVIEW with the vision development module and vision acquisition software (v2017, National Instruments, Austin, TX, USA) in Microsoft Windows. The software development kits (SDK) provided by the manufacturers of the camera and LCTF were used to operate the camera and control the LCTF. The SDK for the camera includes a set of LabVIEW-VIs, which facilitate the selection of exposure time, trigger mode to synchronize the camera exposure with other processes, image binning and ROI selection, image format options, amongst other settings. Likewise, the LCTF's SDK contains sub-VIs for wavelength selection, control mode options, and LCTF status monitoring. Although the LCTF controller provides the option of external triggering using a 5 V transistor-transistor logic signal or analog signals to trigger the controller to switch the wavelength, in this work the controller was programmatically triggered and synchronized with the camera exposure time.

The LCTF has an optimal operating temperature of 40°; if the temperature is too low or high, the passband wavelength might be shifted and the waveband switching speed slower. Therefore, the temperature was programmatically monitored in real time to guarantee the performance and safety of the system. In addition, the camera temperature was also monitored while operating. If the temperature of either the camera or LCTF exceeded the programmatically defined limit, a warning message was displayed and the imaging system automatically moved to an idle state until temperature returned to normal.

The developed software interface facilitates data collection in three different modes. In hyperspectral imaging mode, the user can input the wavelength range and the waveband interval to collect a complete hypercube of the scanned samples. For acquiring selected band images, the multispectral imaging function can be chosen and the user should specify the wavelengths and the number of wavebands (minimum 2 wavebands). Furthermore, the selected wavelength range for the hyperspectral imaging mode and the wavelengths for the multispectral imaging mode can be saved. The single waveband option collects and saves a specified single waveband image. The collected images via any of the above three models can be saved in TIFF format using a defined filename and save path. The collected waveband image is displayed on the image window, and can be previewed by checking the preview

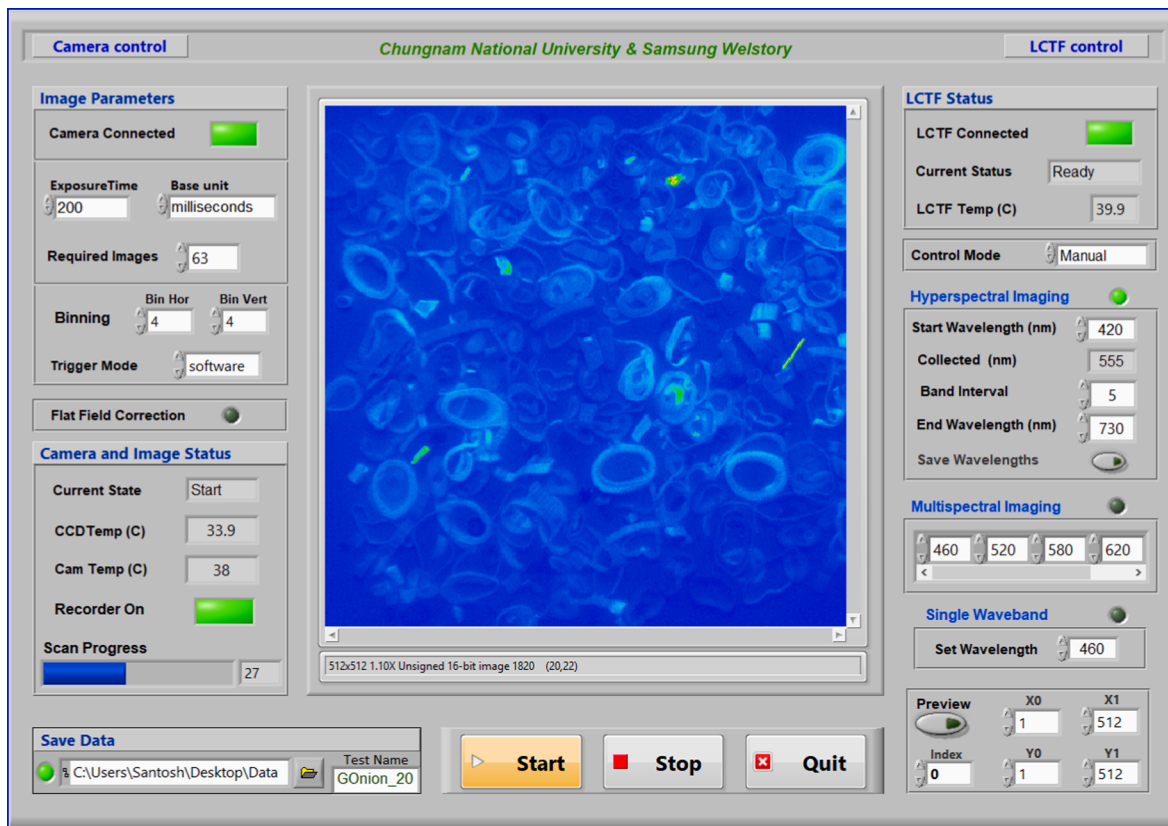


Fig. 3. Software interface for system control and image acquisition.

option.

2.4. System calibration

In order to achieve the best possible performance from the LCTF-based imager, it should be calibrated in both spectral and spatial domains. Since the LCTFs are well calibrated in the spectral domain by the manufacturers and previous reports show a maximum of 2 nm deviation of measured peaks from the claimed peaks by the manufacturers (Markstrom & Mabbott, 2011; Wang et al., 2012b), we chose not to calibrate in the spectral domain. Moreover, the level of calibration required by an instrument is dependent on the application. Some applications, as in our case, only require self-consistent data and would only require that the instrument provides results that are reproducible (Allen et al., 2007). However, the system was calibrated in the spatial domain for spatial resolution, FOV, and image distortion. The different band images of a piece of black and white striped paper were collected. Under the desired settings, the calculated and measured image line length and spatial resolution showed a perfect match. Furthermore, the FOV of the system was measured by collecting the images of the white striped paper by changing the image distance of the object from 30 to 110 cm in 10 cm increments. The calculated and measured FOV showed a perfect linear relationship. In order to check any image distortion, reflectance images of a color checker board at different wavebands, as shown in Fig. S1, were collected. The different band images were then overlapped with each other to match the color square points. However, no image distortion was observed visually. In addition, from the band images, it could be seen that the different band images showed different color intensities of the respective color squares; for instance, the band images of 450 nm, 520 nm, and 695 nm showed high intensity for blue, green, and red squares, respectively.

2.5. Fresh-cut samples and foreign materials

Two different kinds of fresh-cut vegetables, namely, cabbage and green onion samples (Fig. S2 and S3) were provided by a fresh-cut processing unit in Daejeon (South Korea). These two fresh-cut vegetables were considered for this study because of their different response to fluorescence and variation in color; for example, cabbage samples are light green and whitish in color, but green onion samples show significant color variation from dark green to light green, yellowish white to clear white, etc. Thus, the fluorescence spectra and color intensities vary with color variation.

A wide range of materials representing those that could be accidentally added to the fresh-cut vegetables were provided by the same processing company. These FMs are shown in Fig. 4, and include transparent and colored plastic pieces, peel residues, different kind of insects, small metal pieces, and different kind of woods pieces, including raw woods (in dark color) and processed woods, such as from toothpicks and earbuds. In addition to these, a range of other foreign materials were also considered and will be discussed later.

2.6. Online detection system design

Fig. 5 shows a schematic diagram of the online sensing system for foreign material detection in fresh-cut vegetables. The system comprises the aforementioned LCTF-based imager and UV-A (365 nm) illumination source, a color camera and two side-by-side rows of 7.2 W white LEDs (SS LIGHT, South Korea) inside a dark chamber, conveyor unit, stepper motor, motion controller board, and a computer unit. Since fluorescence imaging by the LCTF-based imager is theoretically sensitive only to the fluorescence of foreign materials, a color camera was installed to capture the RGB imaging of the same scene for detection of colorful foreign materials. The color camera was a 5-megapixel CMOS camera (Hikvision, MA, USA) incorporated with an objective lens of 25

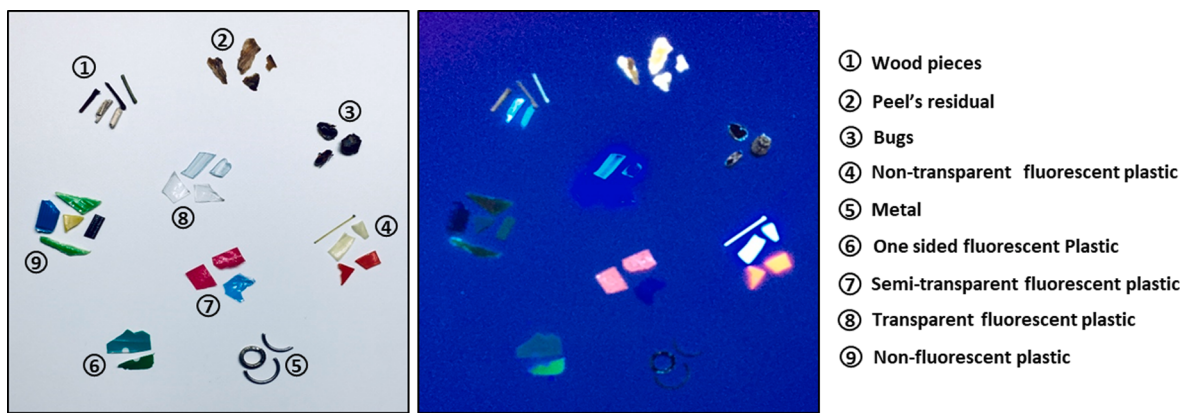


Fig. 4. Digital photograph of foreign materials taken with color camera illuminated with white LEDs (left) and UV-A (365 nm) illumination (right).

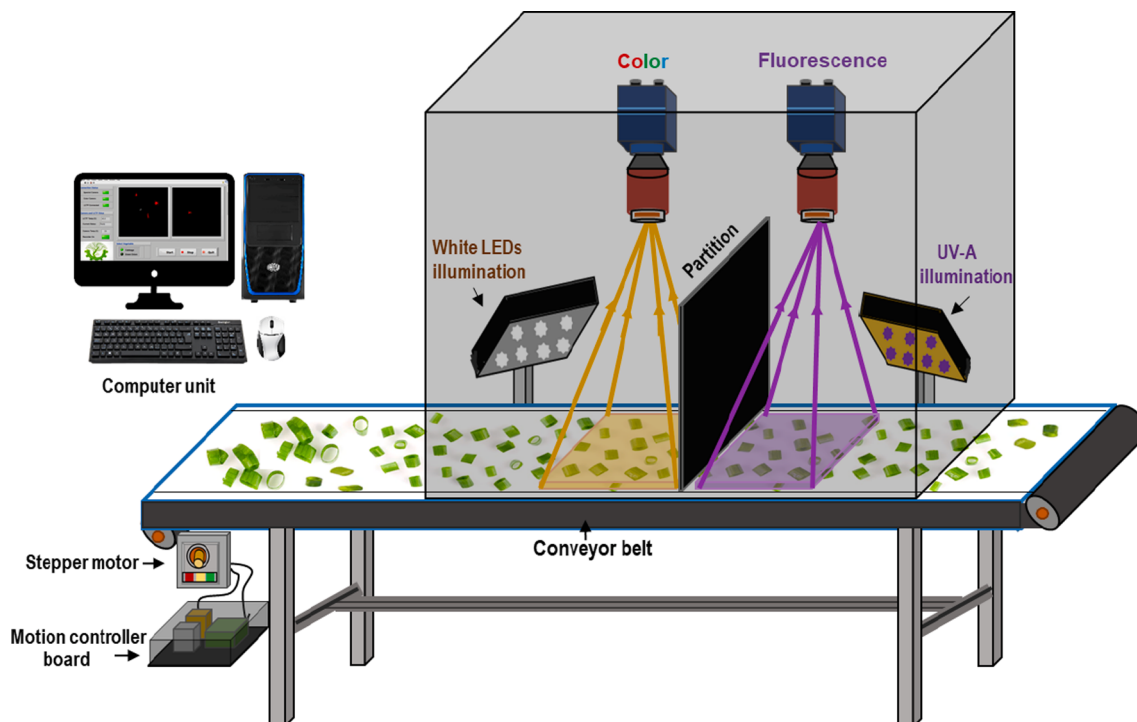


Fig. 5. Schematic of LCTF-fluorescence imager and color camera-based online detection system.

mm focal length. The color images of samples on the conveyor unit were collected by white LED illumination. These two sensing units (fluorescence and color imaging) were separated in two compartments by a 5 mm thick dark board partition so that the illumination from the white

LEDs (for color imaging) did not interfere with fluorescence imaging (UV-A illumination), and vice versa.

In this work, a white colored conveyor belt constructed from polyester urethane materials was used. The selection of the conveyor belt

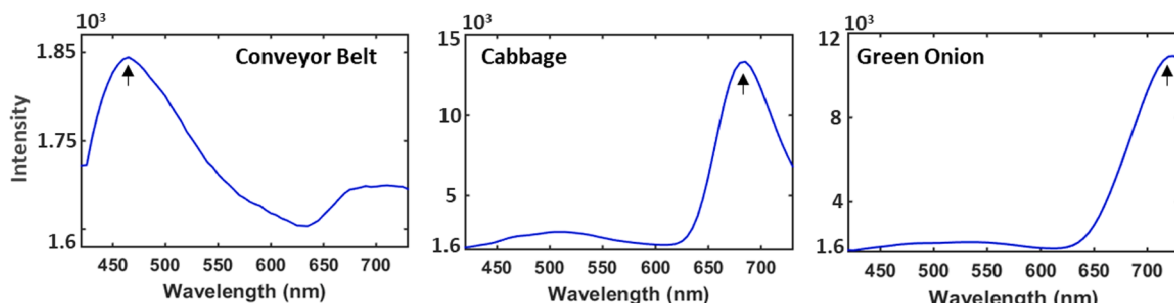


Fig. 6. Fluorescence spectra of conveyor belt and cabbage and green onion samples extracted from the hypercube acquired using the developed LCTF-based spectral imaging system. (For interpretation of the references to color in this figure legend, the reader is referred to the web version of this article.)

was based solely on its color and fluorescence characteristics because commonly occurring white-colored foreign materials, such as pieces of A4-size paper and tissue paper, can be detected by fluorescence imaging owing to their high fluorescence signals. Conversely, by using a conveyor belt of any other color (i.e., green, blue, black etc.), similarly colored non-fluorescent foreign materials could be missed because they cannot be separated from the conveyor unit using color imaging nor detected using fluorescence imaging. In addition, the fluorescence characteristics of the (polyester urethane) conveyor belt show a strong fluorescence peak around 465 nm, as shown in Fig. 6. Thus, for a 465 nm fluorescence band image, non-fluorescent foreign materials on the conveyor belt will show relatively lower fluorescent intensity compared to the fluorescent intensity of conveyor belt, and thus can be detected.

A step motor (Ezi Servo ST, Fastech, Korea) was used with a National Instruments (NI) motion controller (PCI-7334) to run the conveyor in a ‘stop-go-stop’ mode from fluorescence to color imaging chamber. The conveyor belt movement was programmatically controlled and synchronized with the sensing units in such a way that the fluorescence images of samples on the conveyor unit were collected first, and the color images of the same area were acquired after the samples move a step (~24 cm) forward to the FOV of the color camera. It should be noted that instead of using a speed- or torque-specific step motor, a position-specific step motor was used to position the samples accurately from one chamber to another (fluorescence to color imager) throughout the whole system operation.

2.7. Image acquisition and analysis

All images of foreign materials and fresh-cut vegetables were acquired using both fluorescence imaging and the color camera. Six individual test sets were prepared for each fresh-cut vegetable. In test set-1, non-fluorescent FMs, including metal pieces, insects, non-fluorescent plastic, and wood pieces, were mixed with fresh-cut vegetables. Only fluorescent FMs were mixed with fresh-cut vegetables in test set-2. To check the repeatability, both test sets-1 & 2 were scanned twice. Fig. 4 shows an easy assessment of fluorescent and non-fluorescent foreign materials used in this work. The other four test sets included both fluorescent and non-fluorescent FMs in fresh-cut vegetables and each were scanned once.

The fluorescence and color images of FMs with mixed fresh-cut vegetables were collected for each test set. The fluorescence images were first collected by arranging samples onto the conveyor unit and illuminating by UV-A light source as shown in Fig. 5. The FOV of the LCTF-based fluorescence imager was $24 \times 24 \text{ cm}^2$ when the imager was mounted at a height of 82 cm above the conveyor belt, and the nominal pixel size was 85 μm . The fluorescence data were collected throughout the whole spectral range from 420 to 730 nm with a 5 nm band interval using an exposure time of 150 ms. A spatial binning of 4×4 resulted in a hypercube of $512 \times 512 \times 63$ (512×512 image size and 63 bands). Furthermore, the RGB images of the same area were collected by programmatically moving the conveyor unit (24 cm) toward the FOV of the color camera. The samples were illuminated by white LEDs and CCD exposure time was set at 10 ms to obtain the optimal image quality. The collected hypercube from LCTF-based fluorescence imaging and captured images from the color camera were saved for further analysis.

The principle goal of this study was to develop a fluorescence and color imaging-based online system for rapid detection of foreign materials in fresh-cut vegetables. Thus, the two major aspects of data analysis strategy were (1) selection of the optimal wavebands to reduce the data dimension and thus reduce the data collection and computation time, and (2) keeping the image processing algorithms simple to facilitate real-time image analysis. Therefore, the optimal wavebands for fluorescence imaging were selected initially by visual assessment of extracted fluorescence spectra of each vegetable (cabbage and green onions) and FMs. Firstly, the spectral bands that were considered optimal were selected based on the emission maxima of the vegetables,

conveyor belts, and fluorescent foreign materials. Further, a simple but effective image processing algorithm was developed for analysis of the selected fluorescence band and color images, which utilized the image ratio and image summation, as well as subtraction and simple image thresholding. The image processing flowchart for both fluorescence and color image analysis is shown in Fig. S4.

The LCTF-based collected spectral images could be affected by vignetting because of the non-uniform transmission efficiency of the LCTF. Moreover, the vignetting pattern could be different on different band images, as evident from Fig. S5, as well as non-uniformity caused by a single tilted illumination unit. Thus, vignetting should be removed from the images prior to subjecting them to further data analysis. In this work, an in-built function VI in LabVIEW was used for vignetting correction purposes; the equation used for vignetting correction and vignetting-corrected images are shown in Fig. S5. All selected band images were subjected to vignetting correction prior to any data analysis. However, no such vignetting effect was observed in color images.

3. Results and discussion

3.1. Fluorescence characteristics of conveyor belt, fresh-cut vegetables, and foreign materials

Because plastic pieces are one of the most frequently occurring foreign materials in fresh-cut vegetables (Edwards & Stringer, 2007), the fluorescence technique takes advantage of the polymer-specific nature of intrinsic fluorescence induced by photoexcitation. It should be noted that some widely used commercial plastics contain additives with a significant fluorescence emission, such as optical brighteners. The fluorescent plastic (polymer) foreign materials used in this study were made from polyethylene terephthalate (PET), polypropylene (PP), polypropylene-isotactic, nylon, and acrylonitrile-butadienestyrene copolymer (ABS). However, non-fluorescent plastics are made from polyethylene (PE), PP, olefin, low density polyethylene (LDPE), and black-coated nylon. All of these polymers (plastics) were identified by FT-IR reference spectra. The FT-IR spectra of all plastic foreign materials were recorded on a Nicolet 6700 (Thermo Scientific Co.) FT-IR spectrometer, configured with an attenuated total reflectance sampling technique. All the recorded spectra were then compared with the spectral library (Hummel Polymer and Additives, Polymer Laminate Films) to verify the polymer type.

The fluorescence characteristics of a range of conveyor belts made from different materials and with different colors (green, blue, white, black, etc.) were initially tested. However, in order to detect the non-fluorescent foreign materials on a conveyor unit during fresh-cut vegetable processing, the conveyor belt should have fluorescence characteristics so that the non-fluorescent foreign materials can be discriminated based on the fluorescence intensity values. Therefore, a white color conveyor belt made from polyester urethane showing a significant fluorescence intensity around 465 nm (Fig. 6) was used in this study. Moreover, the selected conveyor belt had the advantage of being white for color imaging, as any colorful foreign materials could be detected on the white surface, which would not have been possible in the case of a conveyor belt of any other color.

The fluorescence spectra of fresh-cut vegetables given in Fig. 6 show an intense fluorescence peak centered at 685 nm for cabbage samples and 710 nm for green onion samples. These two peaks are in the red and far-red regions of the visible range, respectively, and arise because of the chlorophyll content of these leafy vegetables. Chlorophyll fluorescence at 680 nm and around 710 nm has been used to elucidate the electron transfer mechanism in the photosynthetic apparatus in plants (Allen et al., 2007; Markstrom & Mabbott, 2011). Likewise, the fluorescence spectra of each FM were extracted from the collected fluorescence hypercube data set and plotted against the wavelength to evaluate their response to UV-A illumination. The fluorescence spectra of only fluorescence sensitive foreign materials are shown in Fig. S6. Most

fluorescent foreign materials have a high intensity peak centered around either 465 nm or 615 nm. However, no fluorescence signals were noticed from other plastics (mentioned previously), insects, metals, or dark wood pieces.

3.2. Selection of optimal wavebands for classification

From the industrial perspective, it is not practical to collect the fluorescence images of samples throughout the whole wavelength range (420–730 nm) because of the aforementioned reasons. Therefore, to reduce the data collection time and the data processing load, optimal wavebands were selected for FM detection in fresh-cut vegetables. Principal component analysis (PCA) and analysis of variance (ANOVA) are the most commonly employed methods for optimal waveband selection to reduce the data dimension (Baek et al., 2014; Mo et al., 2017; Seo et al., 2019). These methods are particularly effective for finding the best pair of wavelengths to classify sample features in two or three groups. However, in our study, a multi-level classification requires the discrimination of the conveyor belt from vegetables and foreign materials (fluorescent, and non-fluorescent) and, furthermore, to discriminate vegetable samples from foreign materials (fluorescent and non-fluorescent). Therefore, the optimal wavebands were simply selected by visually examining the fluorescence spectra of the conveyor belt, FMs, and fresh-cut vegetables.

Based on the fluorescence spectra of the conveyor belt, the highest intensity peak centered at 465 nm was selected. As shown in Fig. S2 and S3, non-fluorescent foreign materials obstructing the fluorescence signals originating from the conveyor belt have a relatively lower intensity and can be discriminated utilizing the 465 nm band image. Similarly, the 675 nm waveband was selected for the cabbage sample and the 710 nm

waveband for green onion analysis because of their highest intensity peaks. As mentioned above, most fluorescent FMs show an intense fluorescence peak at either 465 nm or 615 nm; thus, the fluorescent foreign materials can be detected utilizing these two band images. Because the 615 nm waveband has no serious interference from the conveyor belt or fresh-cut vegetables, this waveband image was considered for fluorescent foreign material detection. However, a problem was encountered when the 465 nm waveband for fluorescent FMs was partially obscured by the fluorescence signals of fresh-cut vegetables, as seen in Fig. S2 and S3. Therefore, this waveband image could cause false-positive results, with some foreign materials and some parts of fresh-cut vegetables having similar fluorescence intensities. To overcome this problem, an additional 435 nm waveband image was utilized where a significant difference can be seen between the fluorescence intensity of FMs and fresh-cut vegetables, unlike with the 465 nm band image. Eventually, considering the relatively low intensity of fluorescent FMs at this band, these two band images (435 nm and 465 nm) were averaged and provided a threshold to visualize the presence of fluorescent foreign materials.

3.3. Fluorescence imaging based detection

The developed algorithm for foreign material detection was firstly tested with test set-1 and 2, detailed in Section 2. Test set-1, which included only non-fluorescent FMs in fresh-cut vegetables, was used for determining an optimal threshold value to differentiate the FMs from fresh-cut vegetables and the conveyor belt background. Furthermore, the threshold value for detection of fluorescent FMs was selected based on test set-2. An optimal threshold value in each case (test set-1 and 2) was determined by considering the lowest number of resulting false-

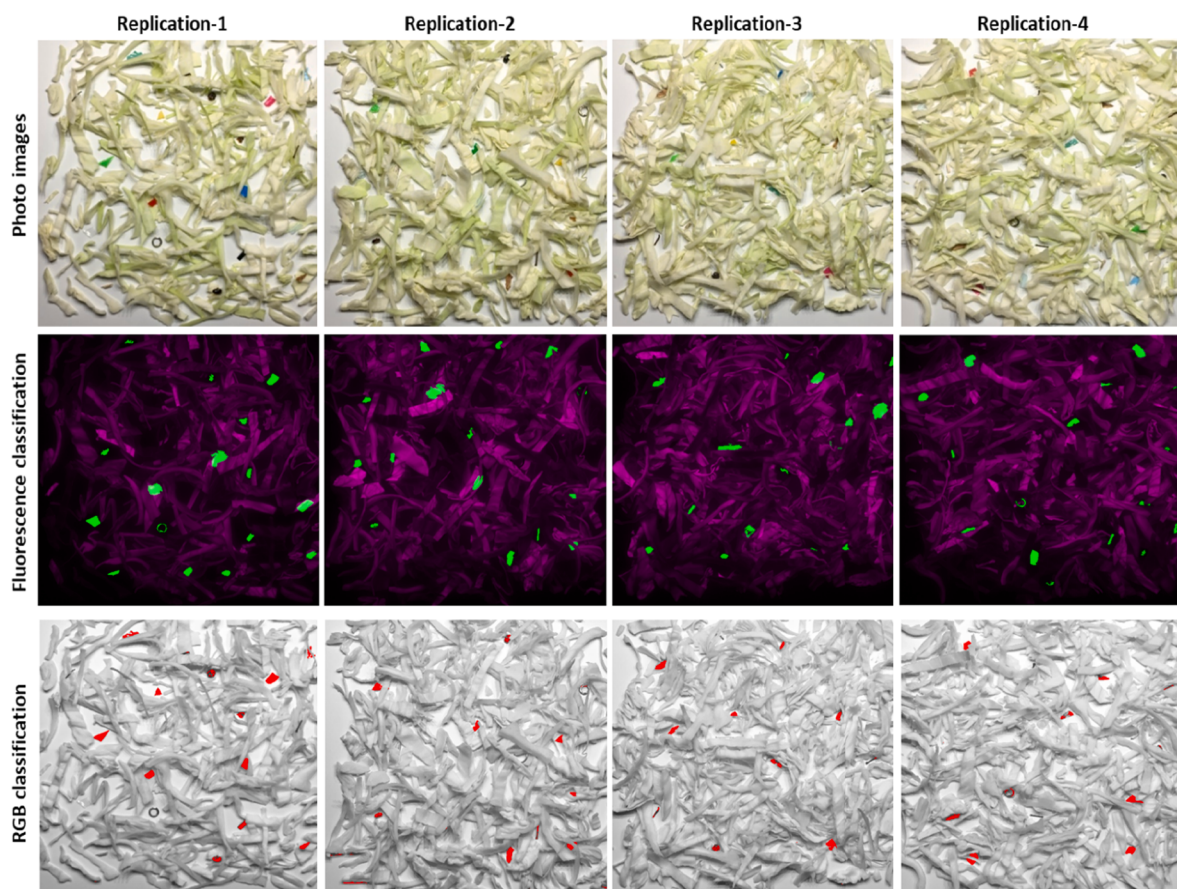


Fig. 7. Color images of foreign materials mixed with cabbage samples (top row), fluorescence-based classification images (middle row), and RGB-based classification images (bottom row).

negative and false-positive pixels. Thus, based on the selected threshold, all FMs mixed with fresh-cut vegetables would be classified correctly with minimal misclassification. Furthermore, the determined threshold values were applied to the processed images of the remaining four test sets of each fresh-cut vegetable (cabbage and green onion), as shown in **Figs. 7 and 8**.

The results of the developed algorithm for FM detection based on the fluorescence images are illustrated in **Fig. 7** (middle row). To visualize the presence and location of FMs, images obtained by global thresholding were combined and overlapped onto the band image of the respective sample. Furthermore, **Tables 1** and **2** list the numbers of accurately detected FMs in cabbage and green onion samples, respectively. The average detection accuracy with the developed LCTF-based fluorescence imaging system was over 85% for both fresh-cut vegetables. It should be noted that all fluorescent FMs, including transparent plastic, thin nylon rods, and small wood pieces, were detected successfully in both fresh-cut vegetables. However, small non-fluorescent foreign materials, such as small pieces of metal, tiny dark wood pieces, and small pieces of yellow and green colored plastic (shown in **Fig. 4**), could not be detected. It should be noted that the single fluorescence illumination unit mounted on the side caused a sample edge effect on the other side, with a fluorescent intensity similar to the intensity of the above non-detected small FMs. Therefore, adjusting the global threshold value (based on test set-1) in order to detect these small non-fluorescent wood pieces introduced a large number of false-positive pixels by classifying the sample edges as foreign materials. The interference effect of sample edges can be mitigated or completely removed by installing two fluorescence illumination units' side-by-side.

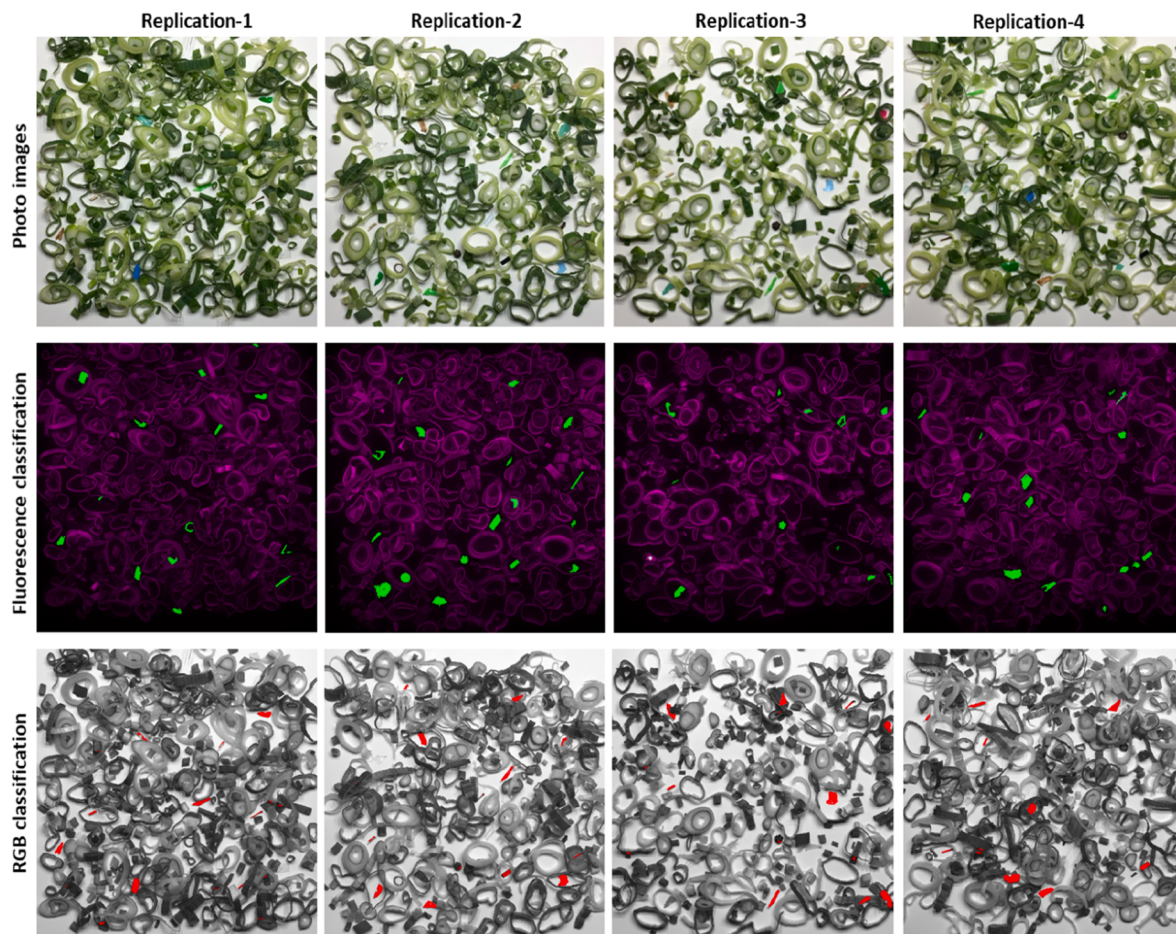


Fig. 8. Color images of foreign materials mixed with green onion samples (top row), fluorescence-based classification images (middle row), and RGB-based classification images (bottom row). (For interpretation of the references to color in this figure legend, the reader is referred to the web version of this article.)

Table 1

Classification accuracy for detection of foreign materials in cabbage samples.

| Replication | Total no. of FMs | Correctly detected | False positive | Accuracy (%) | Combined accuracy (%) |
|-------------|------------------|--------------------|----------------|--------------|-----------------------|
| | | FL/RGB | FL/RGB | FL/RGB | FL + RGB |
| R1 | 19 | 16/12 | 0/0 | 84.2/63.2 | 89.5 |
| R2 | 16 | 15/9 | 0/2 | 93.8/56.2 | 100 |
| R3 | 16 | 14/9 | 1/0 | 87.5/56.3 | 100 |
| R4 | 18 | 16/10 | 0/0 | 88.9/55.5 | 100 |

FMs: Foreign materials; FL: Fluorescence imaging; RGB: Color imaging.

Table 2

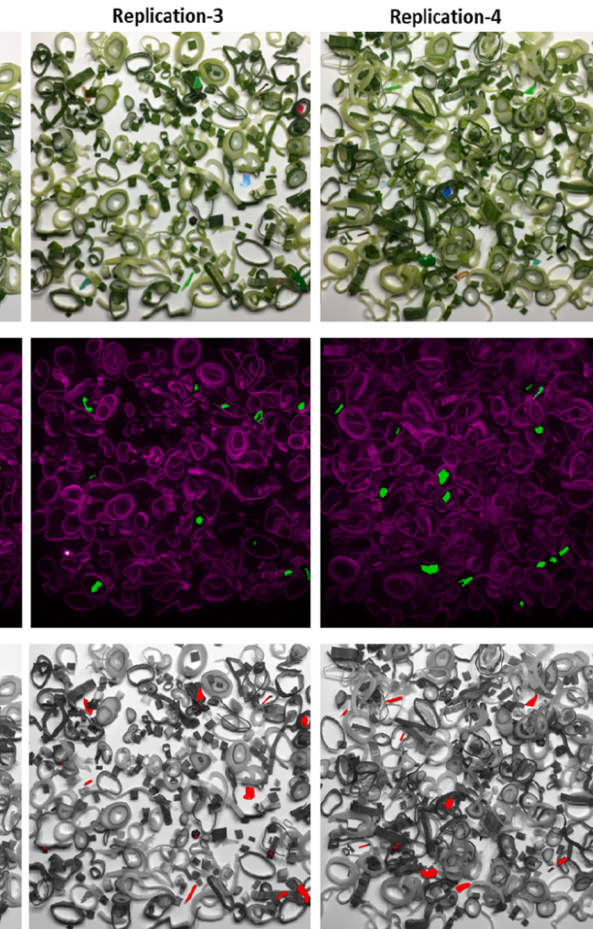
Classification accuracy for detection of foreign materials in green onion samples.

| Replication | Total no. of FMs | Correctly detected | False positive | Accuracy (%) | Combined accuracy (%) |
|-------------|------------------|--------------------|----------------|--------------|-----------------------|
| | | FL/RGB | FL/RGB | FL/RGB | FL + RGB |
| R1 | 16 | 14/10 | 1/3 | 87.5/62.5 | 100 |
| R2 | 19 | 17/12 | 0/1 | 89.5/63.2 | 94.7 |
| R3 | 13 | 11/10 | 0/3 | 84.6/77.0 | 92.3 |
| R4 | 15 | 12/9 | 2/2 | 80.0/60.0 | 93.3 |

FMs: Foreign materials; FL: Fluorescence imaging; RGB: Color imaging.

3.4. Color imaging based detection

Color sorting is not the most reliable method to identify and detect foreign materials in fresh-cut vegetables. However, the idea of using



color imaging here was that any colorful FMs dissimilar in color to the conveyor belt and fresh-cut vegetables could still be detected if overlooked in fluorescence imaging. The acquired images of fresh-cut vegetables shown in [Figs. 7 and 8](#) were subjected to image processing as shown in [Fig. S4](#). Unlike fluorescence imaging, the algorithm was straightforward for processing color images. The color (RGB) image was firstly converted to a gray scale image, and then subtracted from each channel (red, green, and blue). The small FMs of respective colors were then detected by applying threshold values to each subtracted image. An optimal threshold value in each case was determined by considering the lowest number of resulting false-negative and false-positive pixels.

The resulting binary images of foreign materials overlapped onto the red channel images of fresh-cut vegetables are shown in [Figs. 7 and 8](#), and the detection accuracies are summarized in [Tables 1 and 2](#) for cabbage and green onion samples, respectively. From the result tables, it is obvious that the detection accuracy based on color imaging is notably lower than that of fluorescence imaging. The relatively poor detection accuracy is the result of the limitation of color imaging to separate two objects of similar colors; the fresh-cut vegetables tested in this work show a color variation from greenish to white and yellowish in the case of the cabbage samples, and from dark green to light green, white, and light yellow in the case of the green onions. Thus, foreign materials similar in color to these could not be detected by thresholding the color images (intensity), resulting in average accuracy (averaging accuracies for all four replications) of 58% and 65% for detection of FMs in cabbage and green onion samples, respectively.

3.5. Combined fluorescence and color imaging

Although digital imaging devices with three color channels are routinely used for agro-food quality analysis, they cannot uniquely detect foreign materials due to intra-sample (vegetable) color variation. The color discrimination power of color cameras depends on color dissimilarity between the sample and foreign materials. On the other hand, fluorescence imaging enables the recognition of a unique feature for each foreign material and fresh-cut vegetables independently from their chromatic appearance. Non-fluorescent foreign materials can still be detected by using a fluorescent background conveyor belt. However, some foreign materials can still be non-detectable with fluorescence imaging if they exhibit the identical fluorescence features as those of fresh-cut vegetables or small size non-fluorescence FMs are affected by the fluorescence from surrounding objects. Therefore, the combination of fluorescence and color imaging can lead to improved detection accuracy.

[Tables 1 and 2](#) list the fluorescence and color imaging-based combined accuracy for the foreign material detection in fresh-cut vegetables. The results obtained clearly demonstrate the advantage of combining two imaging techniques (fluorescence and color imaging) for detection of foreign materials in fresh-cut vegetables as the combined accuracy in both cases (cabbage and green onion samples) is much higher than the detection accuracy obtained with single imaging technique. The combined accuracy was determined by counting the mutually exclusive detected FMs from the fluorescence and RGB-based classification images. The average detection accuracy of foreign materials in cabbage and green onion samples, calculated by averaging the combined detection accuracy for four replications, surpassed 95%. The dark wood pieces were partially detected in thresholded color images; however, the small metal pieces could not be detected by either fluorescence or color imaging. The obtained results confirm that the detection accuracy can be significantly improved by using a combination of these two imaging techniques.

3.6. Industrial on-site testing

Although impressive at the laboratory scale, most sensing instruments do not perform identically when tested in industrial

environments. Three main factors can influence the performance of laboratory-tested optical sensing units when applied in an industrial environment: (1) environmental factors such as temperature and humidity; (2) lighting effects, including exposure to stray room light; and (3) variation of the physical attributes of samples, such as shape, size, color, and wetness and dryness. Therefore, to achieve the main goal of this work, the sensing unit (LCTF-based imager) was tightly packed inside a custom-designed aluminum frame, and all hardware (including color camera, illumination units, motion controller board, and computer CPU unit) were installed in an enclosed black box as shown in [Fig. 9](#).

A new user-friendly software interface was further developed to collect the multispectral fluorescence and color images by synchronizing both of the sensing units with the conveyor belt movement. The previously developed algorithms for fluorescence and color image processing were then incorporated into the LabVIEW-based software interface. In addition, all the predefined imaging parameters, such as exposure time, image binning, wavelength to be collected, and image processing parameters (e.g., threshold values) were set as constant. The front panel of the software interface is shown in [Fig. 10](#). The software program initially checks and displays the status of the LCTF, spectral camera, and color camera. By pressing the start button, the fluorescence images (four wavebands) of the sample on the conveyor belt ($24 \times 24 \text{ cm}^2$) are firstly acquired. The color images of the same area are then collected by moving the conveyor unit to the FOV of the color camera. The collected fluorescence and color images for samples are processed simultaneously, and detected FMs are depicted in two different image windows (left for fluorescence and right for color imaging in [Fig. 10](#)). The conveyor belt is automatically stopped if any FMs are detected, thus allowing the user to remove the foreign materials manually by confirming their location based on the detection images on the computer monitor. Otherwise, the conveyor belt runs constantly and the fluorescence and color images are collected and processed simultaneously for FM detection until the 'Stop' or 'Quit' button is pressed.

To test the performance of the developed foreign material detection system installed at a fresh-cut vegetable processing unit, the conveyor belt was fed manually with freshly made fresh-cut cabbage and green onion samples. The foreign materials were randomly introduced to the fresh-cut vegetables during their movement through the conveyor belt. In addition to the previously mentioned foreign materials, a range of other potential foreign materials, including HDPE (transparent and of different colors), transparent LDPE, packaging tapes (yellow and brown color), paper (A4-size and tissue paper), rubber bands (yellow and black colors), stones, Styrofoam, and iron (stepper pins and needles) FMs were also tested. By using the previously developed image processing algorithms, most of the above-mentioned foreign materials were detected successfully either by fluorescence or color imaging. However, the transparent LDPE, Styrofoam, small stepper pins, and needles could not be detected. For the effective detection and removal of iron (Fe) foreign materials, we propose the installation of a magnetic rod at some position on the conveyor belt to attract Fe foreign materials while they pass through the magnetic field.

The developed system was tested in an industrial environment for several consecutive days, and it was observed that variations in the physical attributes of samples do not influence the system performance. The developed online detection system can effectively analyze an area of $24 \times 24 \text{ cm}^2$ in about 1.6 s, of which data collection took 600 ms and conveyor belt movement from one position to another took 1 s, while the conveyor belt speed was set as 25 cm/s. It should be noted that the FMs can be effectively detected either on the conveyor belt or in fresh-cut vegetables. However, FMs completely overlapped by fresh-cut vegetable samples will be undetected. A potential limitation of the system for practical (industrial) application would be the non-continuous movement of conveyor unit. Therefore, as a continuation of this work, in the near future our research will focus on installing an automatic feeder in addition to a shaker to support non-continuous (stop-go-stop) movement of the conveyor unit and to lessen the possibility of samples and FMs

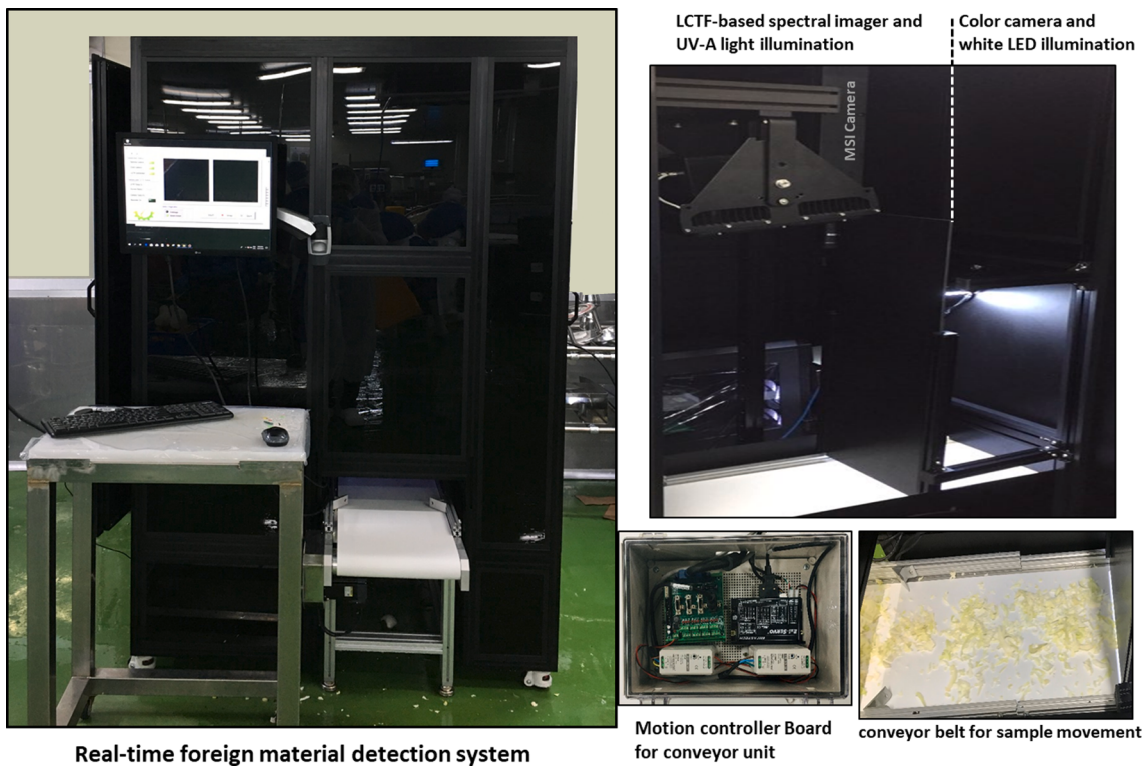


Fig. 9. Photograph of the online detection system installed at a fresh-cut vegetable processing unit for detection of foreign materials using the LCTF-based spectral imager (fluorescence imaging) and color imaging.

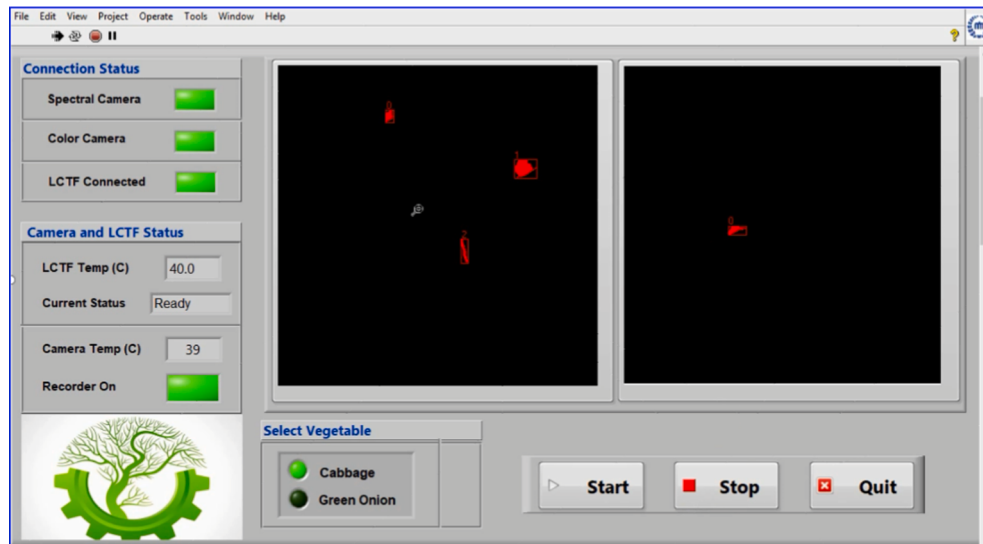


Fig. 10. The user interface for system operation and real-time visualization of detected foreign materials.

overlapping. Moreover, because the developed software provides the coordinates (including the centroids) for each detected FM, installing a robotic arm to remove these detected foreign materials could thus be considered with the interest of our industrial partner.

4. Conclusion

To detect a range of potential FMs in fresh-cut vegetables, a systematic approach was developed using fluorescence imaging in conjunction with color imaging and image processing algorithms. An LCTF-based spectral imager was firstly developed with custom-built

software for imaging system operation and data analysis. The fluorescence images of all fresh-cut vegetables and foreign materials were collected in the 420–730 nm spectral range. For the sake of rapid image collection and analysis, four wavelengths were found to be optimal for potential implementation in rapid and real-time detection of FMs in fresh-cut vegetables. A color camera was installed in conjunction with fluorescence imaging for color imaging-based detection of FMs. All of the hardware, including the LCTF-imager, color camera, and conveyor belt, were programmatically synchronized for simultaneous collection of the multispectral and color images of samples while moving through the conveyor belt. Upon the successful laboratory-based trial of the

developed system, its potential in an industrial environment (at a fresh-cut vegetable processing unit) was evaluated for detection of a wide range of FMs mixed with two kinds of fresh-cut vegetables. The results of this investigation indicate that this technique can be used to effectively detect most potential FMs with high accuracy. Since the potential of the developed online detection system was tested for two types of fresh-cut vegetables, this system has the potential to be extended to other vegetables by selecting the optimal fluorescence wavebands and incorporating a compatible image processing algorithm for each fresh-cut vegetable of interest.

CRediT authorship contribution statement

Santosh Lohumi: Investigation, Methodology, Software, Writing - original draft. **Byoung-Kwan Cho:** Conceptualization, Methodology, Funding acquisition, Writing - review & editing, Supervision. **Sangdeok Hong:** Conceptualization, Data curation.

Declaration of Competing Interest

The authors declare that they have no known competing financial interests or personal relationships that could have appeared to influence the work reported in this paper.

Acknowledgement

This work was supported by Samsung Welstory INC, Republic of Korea.

Appendix A. Supplementary data

Supplementary data to this article can be found online at <https://doi.org/10.1016/j.compag.2020.105912>.

References

- Abdlyat, R., Oreopoulos, J., Sinclair, P., Berman, R., Fang, Q., 2018. High Throughput AOTF Hyperspectral Imager for Randomly Polarized Light. *Photonics* 5 (1), 3. <https://doi.org/10.3390/photonics5010003>.
- Allen, D.W., Litorja, M., Brown, S.W., Zong, Y., 2007. Evaluation of a portable hyperspectral imager for medical imaging applications. *Next-Gener. Spectroscopic Technol.* 6765 (301), 1–10. <https://doi.org/10.1117/12.733189>.
- Baek, I.S., Kim, M.S., Lee, H., Lee, W.H., Cho, B.K., 2014. Optimal fluorescence waveband determination for detecting defective cherry tomatoes using a fluorescence excitation-emission matrix. *Sensors* 14 (11), 21483–21496. <https://doi.org/10.3390/s141121483>.
- Cogdill, R.P., Hurlburgh, C.R., Rippke, G.R., Bakic, S.J., Jones, R.W., McClelland, J.F., Jensen, T.C., Liu, J., 2006. Single-kernel maize analysis by near-infrared hyperspectral imaging. *Trans. ASAE* 47 (1), 311–320.
- Edwards, M.C., Stringer, M.F., 2007. Observations on patterns in foreign material investigations. *Food Control* 18 (7), 773–782. <https://doi.org/10.1016/j.foodcont.2006.01.007>.
- Evans, M.D., Thai, C.N., Grant, J.C., 1998. Development of a spectral imaging system based on a liquid crystal tunable filter. *ASABE* 41 (6), 1845–1852.
- Everard, C.D., Kim, M.S., Lee, H., 2014. A comparison of hyperspectral reflectance and fluorescence imaging techniques for detection of contaminants on spinach leaves. *J. Food Eng.* 143, 139–145. <https://doi.org/10.1016/j.jfoodeng.2014.06.042>.
- Feng, Y.-Z., Sun, D.-W., 2012. Application of Hyperspectral Imaging in Food Safety Inspection and Control: A Review. *Crit. Rev. Food Sci. Nutr.* 52 (11), 1039–1058. <https://doi.org/10.1080/10408398.2011.651542>.
- Francis, G.A., Gallone, A., Nychas, G.J., Sofos, J.N., Colelli, G., Amodio, M.L., Spano, G., 2012. Factors Affecting Quality and Safety of Fresh-Cut Produce. *Crit. Rev. Food Sci. Nutr.* 52 (7), 595–610. <https://doi.org/10.1080/10408398.2010.503685>.
- Gómez-Sanchis, J., Gómez-Chova, L., Aleixos, N., Camps-Valls, G., Montesinos-Herrero, C., Moltó, E., Blasco, J., 2008. Hyperspectral system for early detection of rotteness caused by Penicillium digitatum in mandarins. *J. Food Eng.* 89 (1), 80–86. <https://doi.org/10.1016/j.jfoodeng.2008.04.009>.
- Kim, G.-J., Kim, J.-I., Jeon, S.-G., Kim, J., Park, K.-K., Oh, C.-H., 2012. Enhanced Continuous-Wave Terahertz Imaging with a Horn Antenna for Food Inspection. *J Infrared Milli Terahz Waves* 33 (6), 657–664. <https://doi.org/10.1007/s10762-012-9902-1>.
- Kim, M.S., Lefcourt, A.M., Chen, Y.R., Kim, I., Chan, D.E., Chao, K., 2002. Multispectral detection of fecal contamination on apples based on hyperspectral imagery: Part II. Application of hyperspectral fluorescence imaging. *ASABE* 45 (6), 2039–2047.
- Lapray, P.J., Wang, X., Thomas, J.B., Gouton, P., 2014. Multispectral filter arrays: Recent advances and practical implementation. *Sensors* 14 (11), 21626–21659. <https://doi.org/10.3390/s141121626>.
- LEE, YOUNG.-KI., CHOI, SUNG.-WOOK., HAN, SEONG.-TAE., WOO, DEOG.HYUN., CHUN, HYANG.SOOK., 2012. Detection of Foreign Bodies in Foods Using Continuous Wave Terahertz Imaging. *J. Food Prot.* 75 (1), 179–183. <https://doi.org/10.4315/0362-028X.JFP-11-181>.
- Lu, Y., Lu, R., 2020. Enhancing chlorophyll fluorescence imaging under structured illumination with automatic vignetting correction for detection of chilling injury in cucumbers. *Comput. Electron. Agric.* 168, 105145. <https://doi.org/10.1016/j.compag.2019.105145>.
- Mahesh, S., Manickavasagan, A., Jayas, D.S., Paliwal, J., White, N.D.G., 2008. Feasibility of near-infrared hyperspectral imaging to differentiate Canadian wheat classes. *Biosyst. Eng.* 101 (1), 50–57. <https://doi.org/10.1016/j.biosystemseng.2008.05.017>.
- Markstrom, L.J., Mabbott, G.A., 2011. Obtaining absorption spectra from single textile fibers using a liquid crystal tunable filter microspectrophotometer. *Forensic Sci. Int.* 209 (1–3), 108–112. <https://doi.org/10.1016/j.forsciint.2011.01.014>.
- Mo, C., Kim, G., Kim, M.S., Lim, J., Lee, K., Lee, W.-H., Cho, B.-K., 2017. On-line fresh-cut lettuce quality measurement system using hyperspectral imaging. *Biosyst. Eng.* 156, 38–50. <https://doi.org/10.1016/j.biosystemseng.2017.01.005>.
- Mohd Khairi, M.T., Ibrahim, S., Md Yunus, M.A., Faramarzi, M., 2018. Noninvasive techniques for detection of foreign bodies in food: A review. *J Food Process Eng* 41 (6), e12808. <https://doi.org/10.1111/jfpe.12808>.
- Mustafic, A., Li, C., Haidekker, M., 2014. Blue and UV LED-induced fluorescence in cotton foreign matter. *J. Biolog. Eng.* 8 (1), 1–11. <https://doi.org/10.1186/1754-1611-8-29>.
- Park, B., Yoon, S.-C., Windham, W.R., Lawrence, K.C., Kim, M.S., Chao, K., 2011. Line-scan hyperspectral imaging for real-time in-line poultry fecal detection. *Sens. Instrumen. Food Qual.* 5 (1), 25–32. <https://doi.org/10.1007/s11694-011-9107-7>.
- Seo, Y.W., Lee, H., Mo, C., Kim, M.S., Baek, I., Lee, J., Cho, B.K., 2019. Multispectral fluorescence imaging technique for on-line inspection of fecal residues on poultry carcasses. *Sensors* 19 (16), 1–16. <https://doi.org/10.3390/s19163483>.
- Singh, C.B., Jayas, D.S., Paliwal, J., White, N.D.G., 2009. Detection of insect-damaged wheat kernels using near-infrared hyperspectral imaging. *J. Stored Prod. Res.* 45 (3), 151–158. <https://doi.org/10.1016/j.jspr.2008.12.002>.
- Tutt, J.H., Hall, D.J., Soman, M.R., Holland, A.D., Warren, A.J., Connolley, T., Evagora, A.M., 2014. Comparison of EM-CCD and scientific CMOS based camera systems for high resolution X-ray imaging and tomography applications. *J. Instrum.* 9 (6), 1–14. <https://doi.org/10.1088/1748-0221/9/06/P06017>.
- Wang, W., Li, C., Tollner, E.W., Gitaitis, R.D., Rains, G.C., 2012a. Shortwave infrared hyperspectral imaging for detecting sour skin (*Burkholderia cepacia*)-infected onions. *J. Food Eng.* 109 (1), 38–48. <https://doi.org/10.1016/j.jfoodeng.2011.10.001>.
- Wang, W., Li, C., Tollner, E.W., Gitaitis, R., Rains, G., 2012b. Design and calibration of liquid crystal tunable filter based spectral imaging system. *Am. Soc. Agric. Biolog. Eng. Ann. Int. Meeting* 2012, ASABE 2012, 5, 12, 3625–3642.